Title

Temperature-dependent angle-resolved photoemission spectroscopy study of the Ce 4f states in a possible topological Kondo insulator CeRhAs

Journal

Physical Review B, 102(24)

ISSN

2469-9950

Authors

Seong, Seungho

Kim, Kyoo

Kim, Junwon

et al.

Publication Date

2020-12-01

DOI

10.1103/physrevb.102.245151

Peer reviewed

Temperature-dependent angle-resolved photoemission spectroscopy study of the Ce 4f states in a possible topological Kondo insulator CeRhAs

Seungho Seong,[1] Kyoo Kim,[2,3] Junwon Kim,[2] B. I. Min,[2] T. Takabatake,[4] J. D. Denlinger,[5] and J.-S. Kang[1,*]

[1]*Department of Physics, The Catholic University of Korea, Bucheon 14662, Korea*

[2]*Department of Physics, Pohang University of Science and Technology, Pohang 37673, Korea*

[3]*Korea Atomic Energy Research Institute (KAERI), Daejeon 34057, Korea*

[4]*Graduate School of Advanced Sciences and Engineering, Hiroshima University, Higashi-Hiroshima 739-8530, Japan*

[5]*Advanced Light Source (ALS), Lawrence Berkeley Laboratory, Berkeley, California 94720, USA*

The electronic structure of a possible topological Kondo insulator of CeRhAs has been investigated by employing temperature (T)-dependent angle-resolved photoemission spectroscopy (ARPES). Fermi surfaces (FSs) and band structures are successfully measured for three orthogonal crystallographic planes. The measured Fermi-edge states are found to have a three-dimensional (3D) character, contradictory to the proposed topological surface states of the 2D character. The measured FSs due to the Ce 4f electrons agree well with those from the density functional theory band structures unfolded into the reduced Ce-only unit cell. The theoretically predicted hourglass-type *bulk* bands along $\bar{X}\bar{S}\bar{X}$ are not clearly resolved, in spite of the evident existence of those band features. T-dependent ARPES measurements reveal that the coherent Ce 4f states, having two pseudogap structures of $\Delta_1 \sim 80$ meV and $\Delta_2 \sim 30$ meV, persist to remain above 200 K, in agreement with the high Kondo temperature of CeRhAs.

I. INTRODUCTION

Topological insulators (TIs) possess robust metallic surface states inside a *bulk* energy gap, which are protected by time-reversal symmetry (TRS). They belong to a new quantum phase [1–4]. In topological Kondo insulators (TKIs) of rare-earth (R) 4f systems, the symmetry-protected topological phases are considered to arise from strong correlations [5,6]. In TKIs, the Kondo hybridization between the localized f electrons and conduction electrons (c) leads to the formation of a narrow gap in the bulk bands near the Fermi level (E_F) and the topologically nontrivial band inversion [7–13]. Despite extensive studies on the topological properties of TKIs, the topological nature of 4f electrons is still controversial [12,13].

Other kinds of novel topological Kondo systems [14] have been predicted for isostructural CeNiSn, CeRhSb, and CeIrSb. They belong to the failed Kondo insulators, for which an insulating gap develops due to the Kondo screening and yet a semimetallic phase is stabilized at a lower temperature (T), exhibiting large anisotropy [15–17]. The unique feature of these systems is that they have nonsymmorphic glide and screw-axis symmetries (*Pnma* space group), which bring about exotic Möbius-twisted topological surface states (TSSs) of the hourglass type [14]. These systems are called Möbius Kondo insulators (MKIs). The predicted features of MKIs have not yet been confirmed experimentally [18,19]. Further, it was reported recently that the intriguing hourglass-type bulk band crossings exist around the $\mathbf{k} = S$ point in all three systems [20], which produce the Dirac nodal-loop structures enclosing S in the [100] Brillouin zone (BZ) boundary. These TKIs are expected to display T-dependent topological phase transitions from a potential MKI at low T to a Dirac nodal-loop semimetal at high T. Hence it is very important to investigate the T-dependent behavior of the coherent Kondo states and to identify such hourglass-type bulk band crossings experimentally.

It was found that a crucial factor for the clear observation of the TSS in a potential MKI is the full bulk insulating energy gap on top of the nonsymmorphic crystal symmetries [18]. CeNiSn and CeRhSb reveal a pseudogap (Δ) of small size ($\sim$4 meV in CeNiSn and 5–30 meV in CeRhSb) [15,21–24]. In contrast, the observed energy gap in isostructural CeRhAs [21,24] is much larger, 100–120 meV. Further, the resistivity of CeRhAs is larger than those of CeRhSb and CeNiSn by an order of magnitude [25,26]. In this respect, CeRhAs would be a more appropriate system than CeNiSn and CeRhSb to explore the Kondo insulating nature as well as Möbius TSSs, if they exist.

In this paper, we have performed T-dependent angle-resolved photoemission spectroscopy (ARPES) measurements for CeRhAs, which is a promising candidate of both an MKI [14] and a Dirac nodal-loop semimetal [20]. We have successfully measured Fermi surfaces (FSs) and band structures for three orthogonal crystallographic planes, which is important because the Möbius TSSs are predicted to be realized only for the (010) surface [14]. We have found that the T-dependent behavior of Ce 4f ARPES is consistent with the high Kondo temperature (T_K) of CeRhAs, suggesting the

*Corresponding author: kangjs@catholic.ac.kr

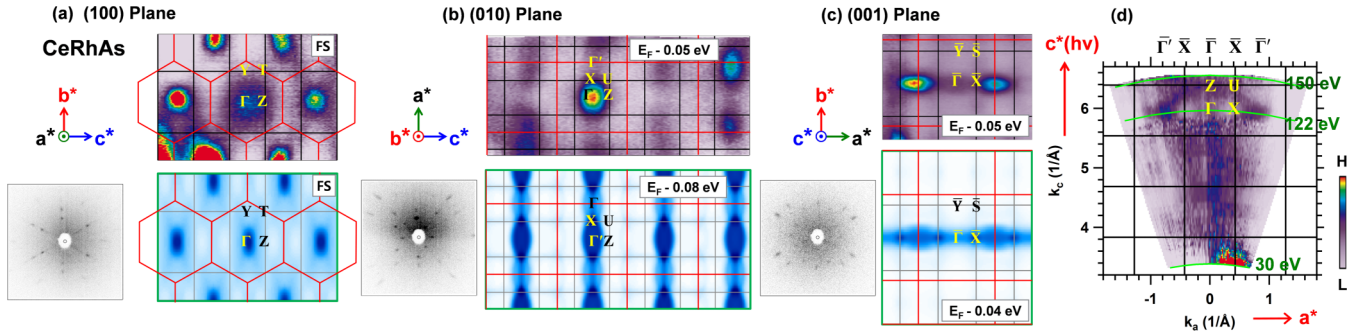

FIG. 1. Fermi surfaces (FSs) of CeRhAs. (a) The measured FS of CeRhAs for the (100) plane (top), in comparison with the DFT FS for the (100) plane (bottom). The data were obtained at the Ce $4f$ resonance ($h\nu = 122$ eV) and at $T = 20$ K. The original orthorhombic BZ is denoted as black lines, and a larger hexagonal BZ is denoted as red lines. The measured Laue pattern for the (100) plane (perpendicular to the a axis) is shown on the left. (b), (c) Similarly for the (010) and (001) planes, respectively, where the red-colored BZs denote those for the smaller Ce-only unit cell (so that the larger BZs). (d) The Fermi-edge state photon-energy ($h\nu$) map for 30 eV $\leqslant h\nu \leqslant$ 150 eV with $h\nu$ along k_c. Here, the BZ is calculated using the inner potential of $V_0 = 18$ eV [32]. See Fig. S1 in the Supplemental Material (SM) for the effect of the inner potential values [35].

importance of the coherent Kondo states in determining the topological properties of CeRhAs.

II. EXPERIMENTAL AND CALCULATIONAL DETAILS

Good-quality single-crystalline CeRhAs samples were prepared by the Bridgman method, as described in Refs. [26,27]. According to the x-ray analysis, the lattice constants are $a = 7.390$ Å, $b = 4.311$ Å, and $c = 7.374$ Å at $T \sim 20$ K [26]. ARPES measurements were carried out at the MERLIN beamline 4.0.3 of the Advanced Light Source (ALS). Single-crystalline samples were cleaved *in situ* using a blade-type cleaver, and measured in vacuum better than 5×10^{-11} Torr and at ~20 K. Fermi energy (E_F) referencing was performed with evaporated gold. A total energy resolution of $\Delta E \approx$ 25 meV was employed at 122 eV photon energy ($h\nu$). The detector 0.1° angular resolution translates to a momentum resolution of $\Delta k < 0.01$ Å^{-1} at 122 eV. FS maps were obtained via polar scans of the sample. In plotting FS maps, the energy window of $E_i \pm 16$ meV was integrated. Band-structure calculations were performed by employing the all-electron fully relativistic density functional theory (DFT) method, implemented in the full-potential local orbital (FPLO) code [28]. The generalized gradient approximation (GGA) scheme is utilized for the DFT exchange-correlation functional [29].

III. RESULTS AND DISCUSSION

In Figs. 1(a)–1(c), the measured FSs and the DFT FSs of CeRhAs are compared for three different planes. All the measured FSs in Figs. 1(a)–1(c) were obtained at the Ce $4f$ resonance ($h\nu = 122$ eV) and at $T = 20$ K. The (100) plane exhibits circular FSs around the Γ points, while those for the (010) and (001) planes exhibit elliptical FSs, elongated along k_a for both cases. The Laue patterns shown at the left, obtained after ARPES measurements, confirm that the measured FSs really represent those of the (100), (010), and (001) planes, respectively.

CeRhAs exhibits a structural transition from the hexagonal to orthorhombic structure below $T = 360$ K [30,31]. The orthorhombic structure is deformed slightly from the hexagonal structure, with the orthorhombic a axis [100] corresponding to the hexagonal c_h axis [18]. In Fig. 1(a), the original orthorhombic BZ is denoted as black lines, and the larger hexagonal BZ is denoted as red lines. Sixfold symmetry is observed clearly in the measured FS for the (100) plane, supporting that the measured surface indeed represents the (100) plane.

Similarly, Figs. 1(b) and 1(c) show the measured and calculated FSs for the (010) and (001) planes, respectively [32]. Note that the symmetric features in the measured FSs in the (010) and (001) planes do not match with those of the orthorhombic BZ (black lines), but they appear to fit with those of the enlarged BZs. Indeed, fairly good agreement is found between the measured and the calculated FSs, where the DFT FSs represent those unfolded into the larger BZ (red-colored BZ) of the reduced Ce-only unit cell [18,33]. Namely, the FS in the (100) plane, exhibiting quasihexagonal symmetry, is described well by the FS unfolded into the larger hexagonal BZ (in red) of the Ce-only unit cell, and those in the (010) and (001) planes [34] also match well with the periodicity of the Ce-only BZ. This is because the measured FSs in Figs. 1(a)–1(c) are obtained at the Ce resonance, so that they are dominated by Ce $4f$ electrons and the contributions from the Rh $4d$ and As $4p$ electrons are negligibly weak [35,36].

Figure 1(d) shows the Fermi-edge state $h\nu$ map, obtained between 30 and 150 eV with $h\nu$ along k_c and $k_\parallel$ along $\bar{X}\bar{\Gamma}\bar{X}$. Here, $\bar{\Gamma}$ and $\bar{X}$ denote the symmetry points in the projected surface BZ. Bulk Γ and Z along [001] are projected onto $\bar{\Gamma}$ and bulk X and U along [001] are projected onto $\bar{X}$. An elliptical FS centered around $\bar{\Gamma}$ is observed, indicating the three-dimensional (3D) character of the E_F states. Hence, Fig. 1 reveals that the E_F states in CeRhAs have a 3D character. These findings are inconsistent with the theoretically predicted Möbius-twisted TSSs of a 2D character [14]. Note, however, that the existence of the Möbius-twisted TSSs is not ruled out completely if the bulk energy gap is much smaller than the energy resolution of our ARPES data ($\Delta E \approx$ 25 meV).

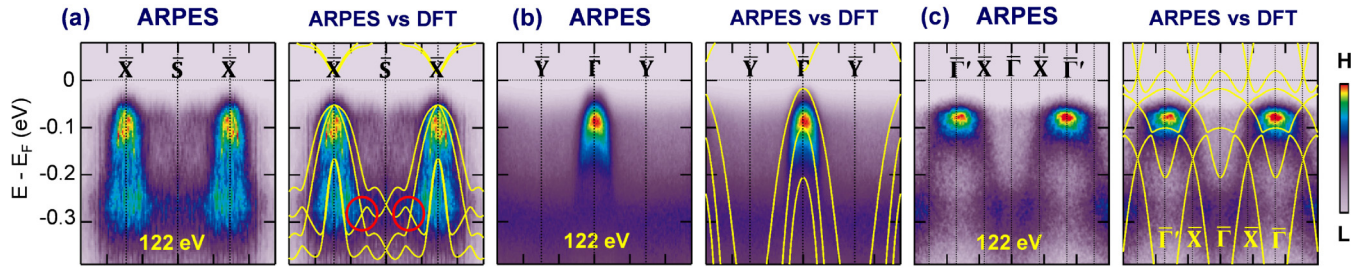

FIG. 2. (a) Left: ARPES image plot of CeRhAs along $\bar{X}\bar{S}\bar{X}$, obtained with $h\nu = 122$ eV. Right: Comparison between ARPES and DFT bands. (b), (c) Similarly along $\bar{Y}\bar{\Gamma}\bar{Y}$ and $\bar{X}\bar{\Gamma}\bar{X}$, respectively. In the comparison between ARPES and DFT, all the DFT bands are shifted by -20 meV. Details of the comparison are shown in Fig. S2 of SM [35]. In (a), red circles denote the hourglass-type bulk band structures in the calculated band structures.

Figures 2(a)–2(c) show the measured ARPES image plots along $\bar{X}\bar{S}\bar{X}$, $\bar{Y}\bar{\Gamma}\bar{Y}$, and $\bar{X}\bar{\Gamma}\bar{X}$, respectively, which are compared with the DFT bands along XSX, $Y\Gamma Y$, and $X\Gamma X$, respectively. The process of the comparison is shown in Fig. S2 of SM [35]. ARPES data were obtained at the Ce $4f$ resonance ($h\nu = 122$ eV). Here, the symmetry line along $\bar{X}\bar{S}\bar{X}$ is chosen in order to observe the hourglass-type bulk band structures in CeRhAs [20]. At low T below the Kondo coherence temperature $T_{\rm coh}$, the hourglass-type bulk band structures are predicted to be located well below $E_{\rm F}$, so that it will be easier to observe them experimentally than to observe the Möbius-twisted TSSs that might exist within the very small bulk energy gap near $E_{\rm F}$.

The flat spin-orbit (SO) sidebands of Ce $4f$ states are observed at ~ -0.3 eV. Then the dispersive bands are observed, which are centered at $\bar{X}$ along $\bar{X}\bar{S}\bar{X}$, at $\bar{\Gamma}$ along $\bar{Y}\bar{\Gamma}\bar{Y}$, and at $\bar{\Gamma}'$ along $\bar{X}\bar{\Gamma}\bar{X}$, corresponding to the holelike FS around $\bar{X}$, $\bar{\Gamma}$, and $\bar{\Gamma}'$, respectively. The different band slopes indicate different effective masses. Excluding the flat Ce $4f$ states at ~ -0.3 eV in ARPES, which are missing in DFT calculations, they reveal reasonably good agreement along $\bar{X}\bar{S}\bar{X}$ and $\bar{Y}\bar{\Gamma}\bar{Y}$. Nonetheless, the hourglass-type bulk bands along XSX (denoted as red circles) are not resolved clearly in ARPES, contrary to our expectation. On the other hand, the energies and the slopes of the several bands along XSX in DFT calculations reveal the overall agreement with ARPES, suggesting that the calculated bands indeed exist in ARPES. But they appear to be smeared out and are not resolved in ARPES, which can be due to the nonflat surfaces in our ARPES measurements or due to the large lifetime broadening.

We now discuss the T dependence of Ce $4f$ states in CeRhAs in Fig. 3, where all the data were obtained along $\bar{X}\bar{\Gamma}\bar{X}$ at the Ce $4f$ resonance. Figure 3(a) shows the T-dependent angle-integrated energy distribution curves (EDCs). Note that a strong $4f$ Kondo peak is observed well below $E_{\rm F}$ ($\sim$80 meV below $E_{\rm F}$), reflecting a pseudogap in the Ce $4f$ states. This feature will be discussed further in Fig. 4. The additional broad feature at -0.3 eV represents a final-state SO sideband of $4f$ character. Interestingly, with increasing T up to $\sim$200 K, the Kondo peak does not disappear, although its intensity decreases. This behavior is highlighted by plotting the ARPES images for several selected temperatures in Fig. 3(b). At low T, strong $4f$ peaks are observed at $\bar{\Gamma}'$ at ~ -80 meV. With increasing T, the f amplitudes decrease slightly, but the $4f$ peaks do not disappear up to $\sim$200 K, in agreement with the behavior in Fig. 3(a).

Such T dependence is verified in the momentum distribution curves (MDCs) of the $4f$ states, which are presented as an image versus T in Fig. 3(c) as well as the line cuts in Fig. 3(d). These MDCs manifest that the coherent f states exist up to $T \sim 200$ K, implying $T_{\rm coh}$ for CeRhAs $\geqslant 200$ K. In other words, the coherent Ce $4f$ states remain at least up to $\sim$200 K, making a sharp contrast with that of isostructural CeRhSb that belongs to the original MKI candidates [18]. In CeRhSb, sharp f peaks disappear around $T_{\rm coh} \approx 100$ K. These differences in T-dependent ARPES for CeRhSb and CeRhAs are consistent with the much higher T_K of CeRhAs ($T_K \sim 1200$–1500 K) [21,24] than that of CeRhSb ($T_K \sim 60$–100 K) [15,23,24]. Hence, this finding supports that the coherent Kondo states play a crucial role in determining the topological properties of CeRhAs.

Figure 4(a) shows the angle-integrated valence-band PES spectra of CeRhAs, obtained at the Ce $4f$ resonance ($h\nu = 122$ eV) and away from the Ce $4f$ resonance ($h\nu = 90$ eV), respectively. At the Ce $4f$ resonance, the Ce $4f$ electron emission is dominant over Rh $4d$ and As $4p$/Sb $5p$ electron emissions [35,36]. This comparison shows clearly that Ce $4f$ states are located near $E_{\rm F}$ while most of the Rh $4d$ states are located around ~ -2 eV. Figure 4(b) compares the valence-band PES spectra of CeRhAs and CeRhSb, obtained at $h\nu = 122$ eV. Both of them exhibit the Kondo peak near $E_{\rm F}$ and the SO sideband peak at ~ -0.3 eV. The Kondo peak in CeRhAs is weaker, broader, and located more deeply than that in CeRhSb.

Figure 4(c) shows the Ce $4f$ PES spectrum of CeRhAs near $E_{\rm F}$, obtained with $\Delta E \approx 20$ meV, compared with the PES spectrum of Au metal as an $E_{\rm F}$ reference. A weight suppression, starting at ~ -80 meV, is observed clearly, but with a finite residual weight at $E_{\rm F}$, suggesting that this weight suppression arises from a pseudogap. Namely, the energy gap opens partially in the k space (not over all the k space). Noteworthy in Fig. 4(e) is the change in the slope around ~ -30 meV.

To show this feature more clearly, we have divided the PES spectra by the Fermi-Dirac (FD) function convoluted with the instrumental resolution, as a rough approximation to the density of states (DOS). Then the FD-divided results for

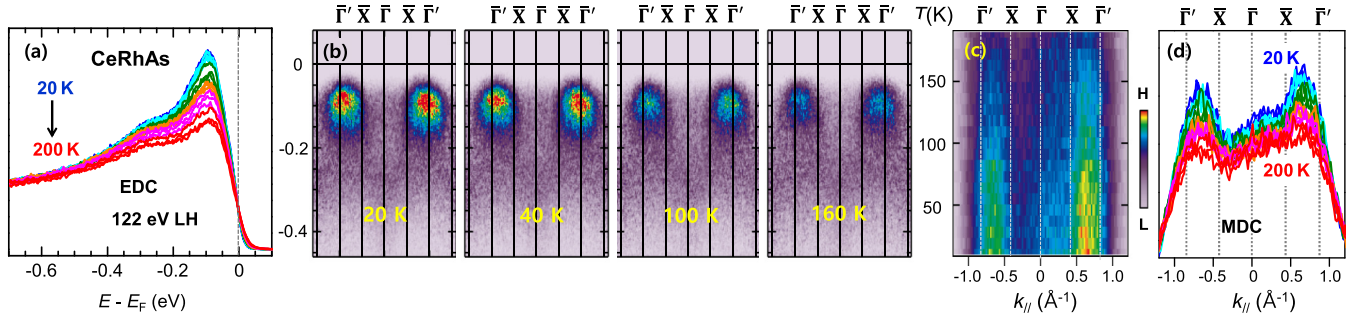

FIG. 3. T-dependent Ce $4f$ states of CeRhAs along $\bar{X}\bar{\Gamma}\bar{X}$. All the ARPES data were obtained at the Ce $4f$ resonance. (a) The integrated Ce $4f$ spectral intensity from 20 to 200 K. (b) ARPES image plots for selected temperatures. (c) MDC images of the E_F states from 20 to 200 K. (d) The E_F-intensity profile of the MDCs from 20 to 200 K.

CeRhAs are symmetrized for the region above E_F. Indeed, the $4f$ DOS in CeRhAs decreases at ~ -80 meV, indicating a pseudogap, in contrast to the flat DOS in Au (see the inset). If we define the pseudogap (Δ) as the energy position for the decrease in the DOS, then $\Delta_1 \sim 80$ meV for CeRhAs, in agreement with the earlier high-resolution PES study [21,22]. But one notices the slope change at ~ -30 meV, which also signifies another pseudogap feature, $\Delta_2 \sim 30$ meV. Hence this FD analysis indicates that there are two energy scales for the pseudogap in CeRhAs, Δ_1 and Δ_2. This feature in CeRhAs makes a sharp contrast to that in CeRhSb [18], where the sharp Kondo peak is located very close to E_F with no pseudogap within the experimental resolution [see Figs. 4(d) and 4(f)]. Note that Fig. 4(f) reveals the increasing slope at E_F in the DOS of CeRhSb, supporting the Kondo resonance peak being located just above E_F so that the observed peak in PES is the tail of the Kondo peak above E_F [37].

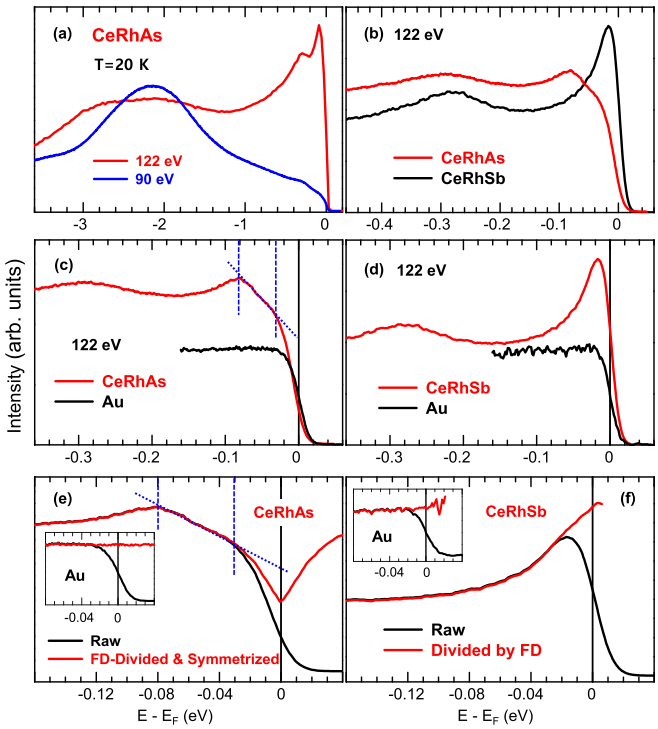

FIG. 4. Angle-integrated valence-band PES spectra of CeRhAs. (a) Comparison of the PES spectra of CeRhAs, obtained at ($h\nu =$ 122 eV) and away from ($h\nu = 90$ eV) the Ce $4f$ resonance, respectively. (b) Comparison of the on-resonance PES spectra of CeRhAs and CeRhSb. (c) The PES spectrum of CeRhAs for the near-E_F region (obtained with $\Delta E \approx 20$ meV), in comparison with that of Au as a Fermi-level reference. Here, dashed lines are guides for the slope change. (d) Similarly for CeRhSb. (e) Comparison of the near-E_F PES spectrum of CeRhAs (black) with that divided by a broadened FD function and then symmetrized for the above-E_F region (red). The inset shows the corresponding PES spectra of Au. (f) Similarly for CeRhSb, for which the above-E_F region is not symmetrized after being divided by an FD function.

Distinctly from CeRhSb and CeNiSn, CeRhAs has a structural transition from hexagonal to orthorhombic at $T =$ 360 K. The existence of the structural transition only in CeRhAs is understood based on its small volume [38]. There has been a longstanding question on the relation between this structural transition and the stability of the energy gap, namely, which one, the structural transition or the f-c band hybridization, governs the gap formation [26,30,31]. It is expected that the structural transition would produce a charge density wave (CDW)-type energy gap, which causes the sudden jump in the resistivity along the b and c directions of the orthorhombic phase [26]. The CDW gaps open at some specific k points on the BZ. We conjecture that the larger pseudogap in ARPES $\Delta_1 \sim 80$ meV corresponds to this CDW gap. Meanwhile, the smaller pseudogap $\Delta_2 \sim 30$ meV in ARPES is thought to arise from the f-c band hybridization. This speculation is supported by the dynamical mean-field theory (DMFT) calculation for hexagonal CeRhAs at $T = 500$ K (Fig. S4 in the SM) [35], which shows coherent f states near E_F, demonstrating that Kondo screening is active already in the high T hexagonal phase.

IV. CONCLUSIONS

In conclusion, we have successfully measured FSs and band structures of a possible TKI of CeRhAs for three orthogonal crystallographic planes. The measured E_F states are found to have a 3D character, distinct from the theoretically predicted Möbius-twisted TSSs of a 2D character. The measured FSs due to Ce $4f$ electrons agree well with the calculated FSs, unfolded to the reduced Ce-only unit cell. The measured band structures along $\bar{Y}\bar{\Gamma}\bar{Y}$ reveal reasonably

good agreement with the DFT calculations. In contrast, the hourglass-type bulk bands along $\bar{X}\bar{S}\bar{X}$ are not resolved clearly. In T-dependent ARPES, coherent Ce $4f$ states persist to remain from low T up to above 200 K, with two pseudogap structures of $\Delta_1 \sim 80$ meV and $\Delta_2 \sim 30$ meV, consistent with the high $T_K \sim 1200$–1500 K of CeRhAs. This finding reveals the importance of coherent Kondo states in determining the topological properties of CeRhAs.

ACKNOWLEDGMENTS

This work was supported by the National Research Foundation (NRF) of Korea (No. 2019R1A2C1004929, No. 2017R1A2B4005175, and No. 2016R1D1A1B02008461), KISTI (Grant No. KSC-2018-CRE-0064), and Internal R&D program at KAERI funded by the MSIT of Korea (Grant No. 524210-20). The ALS is supported by U.S. DOE under Contract No. DE-AC02-05CH11231.

[1] B. A. Bernevig, T. L. Hughes, and S.-C. Zhang, Science **314**, 1757 (2006).
[2] M. König, S. Wiedmann, Ch. Brüne, A. Roth, H. Buhmann, L. W. Molenkamp *et al.*, Science **318**, 766 (2007).
[3] M. Z. Hasan and C. L. Kane, Rev. Mod. Phys. **82**, 3045 (2010).
[4] X.-L. Qi and S.-C. Zhang, Rev. Mod. Phys. **83**, 1057 (2011).
[5] M. Dzero, K. Sun, V. Galitski, and P. Coleman, Phys. Rev. Lett. **104**, 106408 (2010).
[6] M. Dzero, K. Sun, P. Coleman, and V. Galitski, Phys. Rev. B **85**, 045130 (2012).
[7] S. Wolgast, C. Kurdak, K. Sun, J. W. Allen, D.-J. Kim, and Z. Fisk, Phys. Rev. B **88**, 180405(R) (2013).
[8] Z.-H. Zhu, A. Nicolaou, G. Levy, N. P. Butch, P. Syers, X. F. Wang, J. Paglione, G. A. Sawatzky, I. S. Elfimov, and A. Damascelli, Phys. Rev. Lett. **111**, 216402 (2013).
[9] D. J. Kim, J. Xia, and Z. Fisk, Nat. Mater. **13**, 466 (2014).
[10] G. Li, Z. Xiang, F. Yu, T. Asaba, B. Lawson, P. Cai, C. Tinsman, A. Berkley, S. Wolgast, Y. S. Eo, D.-J. Kim, C. Kurdak, J. W. Allen, K. Sun, X. H. Chen, Y. Y. Wangm Z. Fisk, and L. Li, Science **346**, 1208 (2014).
[11] N. Xu, P. K. Biswas, J. H. Dil, R. S. Dhaka, G. Landolt, S. Muff, C. E. Matt, X. Shi, N. C. Plimb, M. Radović, E. Pomjakushina, K. Conder, A. Amato, S. V. Borisenko, R. Yu, H.-M. Weng, Z. Fang, X. Dai, J. Mesot, H. Ding, and M. Shi, Nat. Commun. **5**, 4566 (2014).
[12] B. S. Tan, Y.-T. Hsu, B. Zeng, M. C. Hatnean, N. Harrison, Z. Zhu, M. Hartstein, M. Kiourlappou, A. Sirvastava, M. D. Johannes, T. P. Murphy, J.-H. Park, L. Balicas, G. G. Lonzarich, G. Balakrishnan, and S. E. Sebastian, Science **349**, 287 (2015).
[13] P. Hlawenka, K. Siemensmeyer, E. Weschke, A. Varykhalov, J. Sánchez-Barriga, N. Y. Shitsevalova, A. V. Dukhnenko, V. B. Filipov, S. Gabáni, K. Flachbart, O. Rader, and E. D. L. Rienks, Nat. Commun. **9**, 517 (2018).
[14] P.-Y. Chang, O. Erten, and P. Coleman, Nat. Phys. **13**, 794 (2017).
[15] T. Takabatake, H. Tanaka, Y. Bando, H. Fujii, S. Nishigori, T. Suzuki, T. Fujita, and G. Kido, Phys. Rev. B **50**, 623 (1994).
[16] T. Ekino, T. Takabatake, H. Tanaka, and H. Fujii, Phys. Rev. Lett. **75**, 4262 (1995).
[17] M. Sera, N. Kobayashi, T. Yoshino, K. Kobayashi, T. Takabatake, G. Nakamoto, and H. Fujii, Phys. Rev. B **55**, 6421 (1997).
[18] S. Seong, K. Kim, E. Lee, C.-J. Kang, T. Nam, B. I. Min, T. Yoshino, T. Takabatake, J. D. Denlinger, and J.-S. Kang, Phys. Rev. B **100**, 035121 (2019).
[19] C. Bareille, T.-S. Nam, T. Takabatake, K. Kuroda, T. Yajima, M. Nakayama, S. Kunisada, S. Akebi, M. Sakano, S. Sakuragi, R. Noguchi, B. Il Min, S. Shin, and T. Kondo, Phys. Rev. B **100**, 045133 (2019).
[20] T.-S. Nam, Chang-Jong Kang, D.-C. Ryu, J. Kim, H. Kim, K. Kim, and B. I. Min, Phys. Rev. B **99**, 125115 (2019).
[21] H. Kumigashira, T. Takahashi, S. Yoshii, and M. Kasaya, Phys. Rev. Lett. **87**, 067206 (2001).
[22] K. Shimada, K. Kobayashi, T. Narimura, P. Baltzer, H. Namatame, M. Taniguchi, T. Suemitsu, T. Sasakawa, and T. Takabatake, Phys. Rev. B **66**, 155202 (2002).
[23] S. Nishigori, H. Goshima, T. Suzuki, T. Fujita, G. Nakamoto, H. Tanaka, T. Takabatake, and H. Fujii, J. Phys. Soc. Jpn. **65**, 2614 (1996).
[24] P. K. Misra, *Heavy-Fermion Systems*, Handbook of Metal Physics Vol. 2 (Elsevier, Amsterdam, 2008).
[25] T. Takabatake, G. Nakamoto, H. Tanaka, Y. Bando, H. Fujii, S. Nishigori, H. Goshima, T. Suzuki, T. Fujita, I. Oguro, T. Hiraoka, and S. K. Malik, Physica B **199-200**, 462 (1994).
[26] T. Sasakawa, T. Suemitsu, T. Takabatake, Y. Bando, K Umeo, M. H. Jung, M. Sera, T. Suzuki, T. Fujita, M. Nakajima, K. Iwasa, M. Kohgi, Ch. Paul, St. Berger, and E. Bauer, Phys. Rev. B. **66**, 041103(R) (2002).
[27] P. Salamakha, O. Sologub, T. Suemitsu, and T. Takabatake, J. Alloys Compd. **313**, L5 (2000).
[28] K. Koepernik and H. Eschrig, Phys. Rev. B **59**, 1743 (1999).
[29] J. P. Perdew, K. Burke, and M. Ernzerhof, Phys. Rev. Lett. **77**, 3865 (1996).
[30] K. Umeo, K. Masumori, T. Sasakawa, F. Iga, T. Takabatake, Y. Ohishi, and T. Adachi, Phys. Rev. B **71**, 064110 (2005).
[31] T. Sasakawa, K. Mine, K. Shigetoh, and T. Takabatake, J. Phys. Soc. Jpn. **74**, 3329 (2005).
[32] In determining the inner potential value (V_0), one normally looks for and finds some k_z-periodic features in the ARPES photon-energy ($h\nu$) map(s) either at E_F or at a deeper binding energy (BE). Then one can hypothesize the high-symmetry planes by matching the bulk BZ boundaries, or one can identify the band features that correspond to theory calculations. However, it was difficult to identify high BE Rh d-band dispersions experimentally due to the low Cooper-minimum cross section of Rh $4d$ states amidst the large Ce $4f$ resonance cross section in CeRhAs. Hence, the same inner potential (V_0) value as that for CeRhSb [18] is assumed for $h\nu$ along [100] and [010] ($V_0 = 12$ eV), which yields $h\nu = 122$ eV to be close to the Γ plane. For $h\nu$ along [001], V_0 is chosen by adjusting the symmetric features in the measured $h\nu$ map at E_F to be at the Γ' points, which results in $V_0 = 18$ eV. Note that there is some uncertainty in the V_0 values assumed in this work, as explained above.

[33] W. Ku, T. Berlijn, and C.-C. Lee, Phys. Rev. Lett. **104**, 216401 (2010).
[34] In this comparison, the constant-energy (CE) surfaces are compared instead of the cuts at E_F ($E_i \equiv 0$), where E_i denotes the initial-state energy, i.e., the cuts at slightly deeper E_i's, because of the very weak features of the FS.
[35] See Supplemental Material at http://link.aps.org/supplemental/10.1103/PhysRevB.102.245151 for (i) the effect of the inner potential values (Fig. S1), (ii) the details of a comparison between ARPES and DFT calculations (Fig. S2), (iii) comparison of the calculated atomic photoionization cross sections in CeRhAs (Fig. S3), and (iv) the DMFT band structure of the hexagonal phase of CeRhAs at $T = 500$ K (Fig. S4), which includes Refs. [39,40].
[36] J. J. Yeh and I. Lindau, At. Data Nucl. Data Tables **32**, 1 (1985).
[37] In Fig. 4(f), the FD-divided data for CeRhSb are not symmetrized for the region above E_F because the Kondo peak is expected to be just above E_F.
[38] O. Janka, O. Niehaus, R. Pttgen, and B. Chevalier, Z. Naturforsch., B **71b**, 737 (2016)
[39] K. Haule, C.-H. Yee, and K. Kim, Phys. Rev. B **81**, 195107 (2010).
[40] K. Haule, Phys. Rev. B **75**, 155113 (2007).